



Combination of pre-treatment dynamic [¹⁸F]FET PET radiomics and conventional clinical parameters for the survival stratification in patients with IDH-wildtype glioblastoma

Zhicong Li¹ · Adrien Holzgreve¹ · Lena M. Unterrainer¹ · Viktoria C. Ruf² · Stefanie Quach³ · Laura M. Bartos¹ · Bogdana Suchorska^{3,4} · Maximilian Niyazi^{5,6} · Vera Wenter¹ · Jochen Herms² · Peter Bartenstein^{1,6} · Joerg-Christian Tonn^{3,6} · Marcus Unterrainer⁷ · Nathalie L. Albert^{1,6} · Lena Kaiser¹

Received: 22 March 2022 / Accepted: 3 October 2022 / Published online: 13 October 2022
© The Author(s) 2022

Abstract

Purpose The aim of this study was to build and evaluate a prediction model which incorporates clinical parameters and radiomic features extracted from static as well as dynamic [¹⁸F]FET PET for the survival stratification in patients with newly diagnosed IDH-wildtype glioblastoma.

Methods A total of 141 patients with newly diagnosed IDH-wildtype glioblastoma and dynamic [¹⁸F]FET PET prior to surgical intervention were included. Patients with a survival time ≤ 12 months were classified as short-term survivors. First order, shape, and texture radiomic features were extracted from pre-treatment static (tumor-to-background ratio; TBR) and dynamic (time-to-peak; TTP) images, respectively, and randomly divided into a training ($n=99$) and a testing cohort ($n=42$). After feature normalization, recursive feature elimination was applied for feature selection using 5-fold cross-validation on the training cohort, and a machine learning model was constructed to compare radiomic models and combined clinical-radiomic models with selected radiomic features and clinical parameters. The area under the ROC curve (AUC), accuracy, sensitivity, specificity, and positive and negative predictive values were calculated to assess the predictive performance for identifying short-term survivors in both the training and testing cohort.

Results A combined clinical-radiomic model comprising six clinical parameters and six selected dynamic radiomic features achieved highest predictability of short-term survival with an AUC of 0.74 (95% confidence interval, 0.60–0.88) in the independent testing cohort.

Conclusions This study successfully built and evaluated prediction models using [¹⁸F]FET PET-based radiomic features and clinical parameters for the individualized assessment of short-term survival in patients with a newly diagnosed IDH-wildtype glioblastoma. The combination of both clinical parameters and dynamic [¹⁸F]FET PET-based radiomic features reached highest accuracy in identifying patients at risk. Although the achieved accuracy level remained moderate, our data shows that the integration of dynamic [¹⁸F]FET PET radiomic data into clinical prediction models may improve patient stratification beyond established prognostic markers.

Keywords Radiomics · [¹⁸F]FET PET · Survival · Glioma

Nathalie L. Albert and Lena Kaiser contributed equally to this work.

This article is part of the Topical Collection on Oncology - Brain.

✉ Zhicong Li
lzc1225@163.com

Extended author information available on the last page of the article

Introduction

The inclusion of mandatory molecular markers for diagnosis in the World Health Organization (WHO) Classification of Tumors of the Central Nervous System (CNS) in 2016 and revised in 2021 has led to a more rigid definition of prognostically distinct entities [1, 2]. In particular, the isocitrate dehydrogenase (IDH)-wildtype status is associated with a worse prognosis in adult diffuse astrocytic gliomas [3] and results in the diagnosis of a glioblastoma, WHO grade

4, according to the 2021 WHO classification. Additional predictive markers such as the methylation status of the O-6-methylguanine-DNA-methyltransferase (MGMT) promoter further help to stratify brain tumor patients according to their individual risk profile [4]. However, even within the distinct molecularly defined tumor type of IDH-wildtype glioblastomas, few patients survive several years whereas others remain short-term survivors (STS) and die within the first year, indicating further potential for improvement regarding patient stratification [5]. Balancing aggressive treatment including radiation and chemotherapy with quality of life is critical for patients [6]. Therefore, additional prognostic markers beyond established molecular genetic markers and a stratification of survival beyond the neuropathological classification of brain tumors would be helpful to further improve individual prognostication and guide patient management accordingly.

Molecular imaging using positron emission tomography (PET) with radiolabeled amino acids such as *O*-(2- ^{18}F -fluoroethyl)-L-tyrosine (^{18}F FET) has been applied successfully for the characterization and evaluation of primary brain neoplasms [7–9]. Hence, PET imaging was recommended by the Response Assessment in Neuro-Oncology (RANO) Working Group as useful imaging method in addition to conventional magnetic resonance imaging (MRI) in the clinical management of brain tumor patients [10]. Especially dynamic ^{18}F FET PET has been shown to be helpful for non-invasive tumor classification [11] and for individual prognostication even within defined molecular subgroups [7, 12]. Here, radiomics have recently gained increasing interest as a promising non-invasive tool, where quantitative features are extracted from medical images and combined with clinical and genomic information to establish predictive models [13, 14]. However, up to now, there is no radiomic approach based on dynamic ^{18}F FET PET data which aims to perform survival stratification specifically in patients with an IDH-wildtype glioblastoma, despite being one of the most common and aggressive brain tumors.

Therefore, the purpose of this study was to build and evaluate a prediction model, which incorporates clinical parameters and radiomic features extracted from static as well as dynamic ^{18}F FET PET for an individualized survival stratification in patients with a newly diagnosed IDH-wildtype glioblastoma.

Materials and methods

Patients

The retrospective analysis of PET imaging and clinical data was approved by the institutional review board of the LMU Munich (604–16), and all patients gave written informed

consent before the PET scan. Patients with primary diagnosis of a glioma who received a pre-treatment dynamic ^{18}F FET PET scan at the Department of Nuclear Medicine of the LMU Munich were identified for this retrospective study. The inclusion criteria for analysis were (1) histologically confirmed IDH-wildtype glioblastoma according to the updated 2016 WHO classification [1]; (2) pre-treatment evaluation of a dynamic ^{18}F FET PET scan (ECAT EXACT HR+, Siemens Healthineers, Inc., Erlangen, Germany; Siemens Medical Systems, Inc., Erlangen, Germany); (3) ^{18}F FET-positive glioma (tumor-to-background ratio, TBR ≥ 1.6); and (4) availability of clinical characteristics, including age, gender, Karnofsky Performance Score (KPS), as well as MGMT promoter methylation status and telomerase reverse transcriptase promoter (TERTp) mutation status. Patients with no follow-up data were excluded. Patients with a survival time ≤ 12 months were defined as short-term survivors (STS) [15, 16].

^{18}F FET PET image acquisition

^{18}F FET PET images were acquired on an ECAT EXACT HR+ PET scanner (Siemens Healthineers) with the standard protocol [8, 17] at the Department of Nuclear Medicine of the LMU Munich. Dynamic ^{18}F FET PET images were acquired over 40 as detailed in [14]. If relevant motion was observed in dynamic PET images, a frame-wise correction was performed using PMOD fusion tool (version 3.5; PMOD Technologies, Zurich, Switzerland) after frame-wise checking for motion.

Segmentation of tumor volumes and brain background

The mean background activity was assessed from a large crescent-shaped volume of interest (VOI) in the contralateral healthy hemisphere as published previously [18] and recommended in the Joint EANM/EANO/RANO practice guidelines/SNMMI procedure standards for imaging of gliomas using PET with radiolabeled amino acids [19]. For tumor segmentation, a VOI was delineated with a TBR-threshold of 1.6 in static 20–40 min p.i. summation images as previously described [20].

TBR and TTP image generation

The image values were normalized with the mean background value to generate static 20–40 min p.i. (TBR_{20–40}) TBR images. An in-house developed software described previously by Kaiser et al. [21] (C++ with integration of the ROOT data analysis framework, version 6.22/08, CERN, Switzerland; and ITK segmentation and registration toolkit 4.13.3, National Library of Medicine, National Institutes of

Health, USA) was applied to generate voxel-wise parametric images. For the generation of TTP images, time–activity curves (TACs) were derived from each voxel, which were then classified according to the time frame reaching the peak uptake, i.e., (1) <5 min, (2) 5–10 min, (3) 10–15 min, (4) 15–20 min, (5) 20–30 min, and (6) 30–40 min. TTP analyses excluded the first 2.7 min p.i. to avoid influence from early blood flush [21]. In case of a positive late slope (15–40 min p.i.), the TTP was assigned to group 6.

Radiomic feature extraction

Images were resampled to isotropic voxels using linear interpolation (size 2.03 × 2.03 × 2.03 mm³), then radiomic features were extracted in Python (version 3.8.5) using PyRadiomics (version 3.0.1) [22], which complies with the Imaging Biomarker Standardization Initiative (IBSI) guidelines [23]. The included feature classes were first-order features, shape features and texture features, which were extracted from TBR and TTP images, respectively. No image filters were applied. As previously published, a fixed intensity bin size was set to 0.13 for TBR_{20–40} images, resulting from the average interquartile range divided by 4 [21, 24, 25]. The smallest time frame duration considered in the TTP categories was 5 min, which was used as the fixed bin width for feature extraction from TTP images.

Machine learning pipeline

Before feature selection, a stratified random split was used to assign 70% of the patients to the training cohort (n = 99)

and the remaining 30% to the testing cohort (n = 42), with a balanced distribution of STS and non-STS (P = 0.8654, Pearson’s χ^2 test) and clinical parameters in both groups using the Feature Explorer (FAE) [26]. The independent testing cohort was not involved in the process of model training and used only for model testing. Machine learning including feature selection and model construction was implemented in Python (version 3.8.5) using scikit-learn package (version 0.24.1) [27]. The workflow of the processing pipeline is presented in Fig. 1.

Feature standardization was computed only on the training cohort and then applied to both the training and the testing cohorts. For each feature, the mean value and the standard deviation were calculated. The mean value was subtracted from each individual value, which was then divided by the standard deviation.

Before performance evaluation on the test set, feature selection and model fitting was conducted on the training set. Logistic regression (LR) models were built to predict short-term survival of GBM patients in the testing cohort by fitting selected features on the training cohort. For survival classification, LR was applied in “balanced” mode, which gives higher weight to the minority class and lower weight to the majority class. With this setting, weights are automatically adjusted inversely proportional to class frequencies in the input data to avoid the influence from the imbalance of comparison groups [28]. Considering the small amount of data, the solver “liblinear” was used and the maximum number of iterations was set to 1000 for the solver to converge. The remaining settings of the logistic regression classifier provided within the scikit-learn package were set to default.

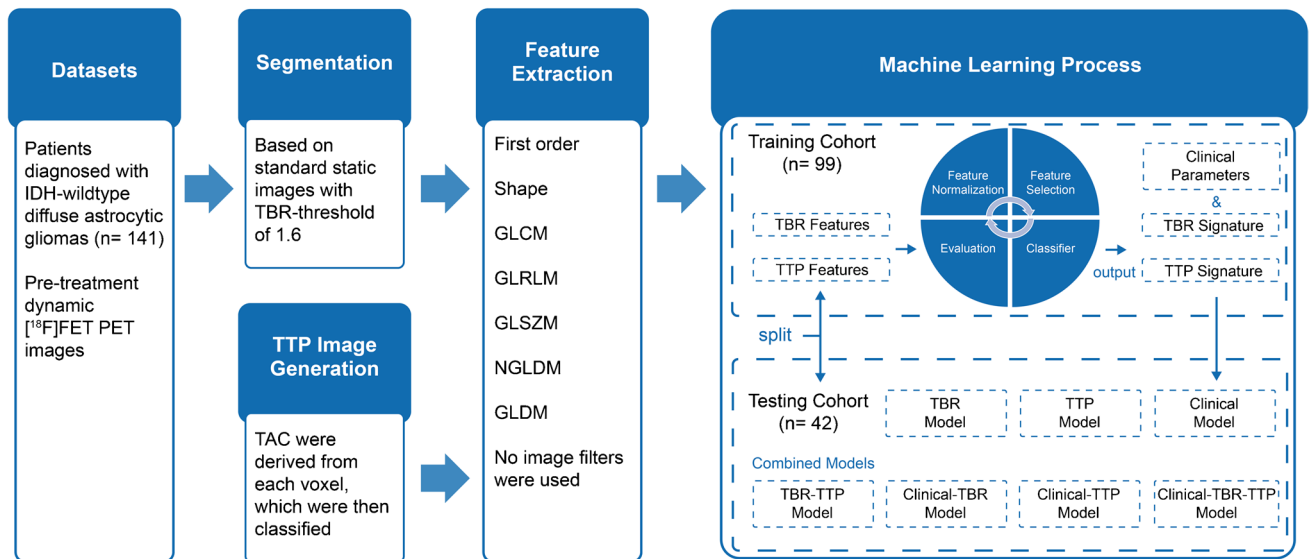


Fig. 1 The workflow of radiomic process. TBR, tumor-to-background ratio; TTP, time-to-peak; TAC, time–activity curves; GLCM, gray level co-occurrence matrix; GLRLM, gray level run length; GLSZM, gray

level size-zone matrix; NGLDM, neighborhood gray level different matrix; GLDM, gray level dependence matrix

Radiomic feature selection

Pearson correlation coefficient (PCC) was used to reduce the dimensions of the feature matrix [29]. The PCC of two features was compared iteratively. If the PCC was larger than 0.99 [30], the second feature was removed. Furthermore, recursive feature elimination (RFE) based on logistic regression classifier was performed to reduce the number of redundant features and select potential survival-related features [31]. During each iteration, a feature which is considered least important is deleted. The number of features to select was chosen to range between 1 and 15. The performance of each model with a different number of features was assessed using the area under the receiver operating characteristic curve (AUC) obtained from repeated stratified cross-validation using three splits and five folds.

Model construction and testing

First, models considering radiomic features derived from either TBR or TTP images or only clinical parameters were generated and compared to each other. Radiomic signatures were generated by using linear combinations of the selected radiomic features according to the LR coefficients in the TBR and TTP models. The clinical model was constructed from all clinical parameters including age, gender, KPS, MGMT promoter methylation status, and TERTp mutation status. Second, the TBR-TTP model was built from a combination of the TBR signature and the TTP signature. The combined clinical-radiomic models were constructed by combining clinical parameters and radiomic signatures, respectively.

Statistical analysis

Receiver operating characteristic curve (ROC) analysis was performed on the training and testing cohorts to evaluate the model performance. AUC, accuracy, sensitivity, specificity, positive predictive value (PPV), and negative predictive value (NPV) were calculated for diagnostic power when applying the trained model on the testing cohort. Then, 95% confidence intervals (CIs) were calculated by using a non-parametric bootstrap method, which was repeated 1000 times to get a bootstrap distribution of the results.

Categorical variables or continuous variables were reported as numbers and percentages or as mean and standard deviation. Categorical variables were compared using Pearson's χ^2 test and continuous variables were compared using Mann–Whitney *U* test. *P* values <0.05 were considered statistically significant.

Statistical analyses were implemented in Python (version 3.8.5) using scikit-learn package (version 0.24.1) [27].

Results

Patient characteristics

A total of 141 patients (median age, 59.3 years; range, 19.0–77.2 years) were included in this study. Of the 141 patients, 94 (66.7%) patients underwent stereotactic biopsy and 47 (33.3%) microsurgical resection at initial diagnosis, with the same distribution between the training and testing cohorts and no significant differences between both STS and non-STS group (*P* value = 0.355). Forty patients (28.4%) had a survival time of less than 12 months and were classified as STS. The variables which constructed the clinical model included age, gender, Karnofsky Performance Score, CNS WHO grade, MGMT promoter methylation status, and TERTp mutation status, and are presented in Table 1. There were no significant differences between the training and testing cohorts with regard to clinical parameters, with STS rates of 28.3% and 28.6%, respectively. The initial therapies of STS and non-STS are shown in Table S1.

Radiomic feature extraction and selection

The original features considered for the model construction included six clinical parameters and 107 radiomic features extracted from static and dynamic [^{18}F]FET PET images, respectively. After the PCC-based exclusion of redundant features, 79 features were retained from TBR images and 94 features were retained from TTP images. With RFE, two features were finally selected for the TBR model and six features for the TTP model (Fig. 2).

Diagnostic validation of the TBR model, TTP model, and clinical model

The TBR model reached an AUC of 0.63 (95% CI, 0.52–0.75) in the training cohort for the prediction of STS (Supplementary Fig. S1a, S1b), with a sensitivity of 60.7% and a specificity of 60.6%, and a similar AUC of 0.63 (95% CI, 0.47–0.78) in the testing cohort, with a sensitivity of 50.0% and a specificity of 73.3%. The TTP model showed a higher predictability of STS (Fig. S1c, S1d) with an AUC of 0.77 (95% CI, 0.69–0.84) in the training cohort (sensitivity 75.0% and specificity 63.4%), and with an AUC of 0.71 (95% CI, 0.57–0.84) in the testing cohort (sensitivity 50.0% and specificity 70.0%). The clinical model demonstrated an accuracy at a comparable level as the TTP model (Fig. S1e, S1f), with an AUC of 0.79 (95% CI, 0.71–0.86) in the training cohort (sensitivity 75.0% and specificity 64.8%) and an AUC of 0.69 (95% CI, 0.50–0.86) in the testing cohort (sensitivity 66.7% and specificity 53.3%).

The coefficients of features in the clinical model are shown in Supplementary Table S2. Radiomic signatures are

Table 1 Clinical characteristics of the patients

Characteristic	Training cohort (n=99)		Testing cohort (n=42)		P value
	STS	Non-STS	STS	Non-STS	
Characteristic	(n=28)	(n=71)	(n=12)	(n=30)	0.865
Age, years	56.7 ± 11.8		58.5 ± 13.1		0.121
Gender					
Female (0)	40 (40.4%)		17 (40.5%)		0.857
Male (1)	59 (59.6%)		25 (59.4%)		
KPS	80 (60–100)		80 (40–100)		0.587
WHO grade					
III	32 (32.3%)		16 (38.1%)		0.640
IV	67 (67.7%)		26 (61.9%)		
MGMT					
Unmethyl. (0)	47 (53.0%)		20 (51.2%)		0.988
Methyl. (1)	52 (47.0%)		22 (48.8%)		
TERTp					
Wildtype (0)	21 (21.2%)		10 (23.8%)		0.516
Mutation (1)	78 (78.8%)		32 (76.2%)		

Data are means ± standard deviations or numbers of patients with percentages in parentheses. P value was derived from the univariate association analyses between each clinical parameter. Calculated by using the Mann–Whitney *U* test for continuous variables and Pearson's χ^2 test for categorical variables. Gender, MGMT, TERTp with representative number of formula of risk probability in parentheses
STS short-term survivors, KPS Karnofsky Performance Score

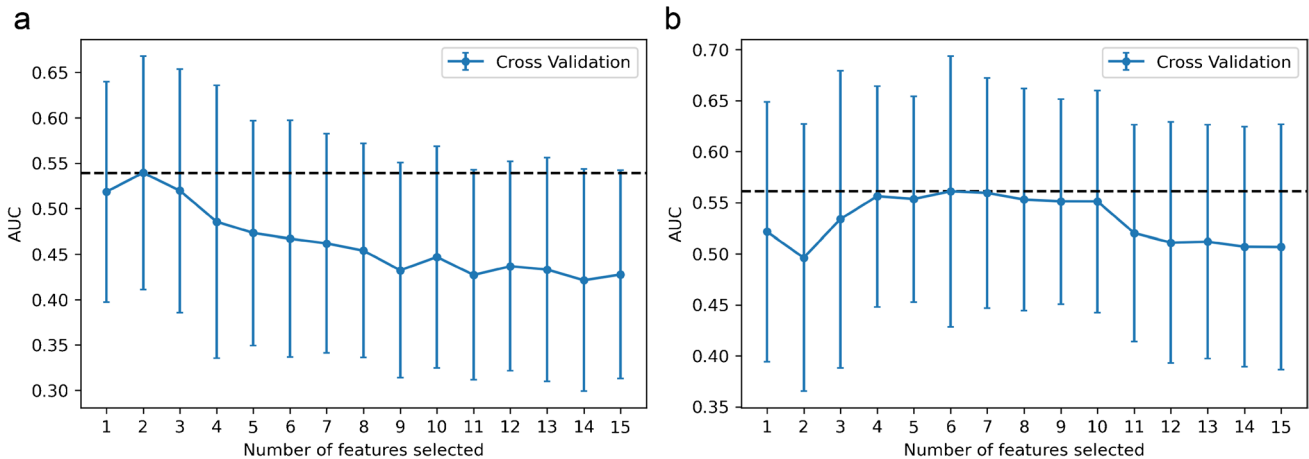


Fig. 2 The feature selection process of the RFE. Each iteration removes a feature that is considered least important and corresponds to a 3-repeated 5-fold cross-validation. After cross-validation, the average AUC of the model in the training cohort was used to determine the optimal number of features. The number of candidate fea-

tures was chosen to range from 1 to 15. The feature number with maximal AUC was selected. **a** Two features were selected in the TBR model and **b** six features were selected in the TTP model. RFE, recursive feature elimination; AUC, area under the receiver operating characteristic curve

provided in Supplementary section S2. Detailed information about the performance of the different models is shown in Table 2 and Supplementary Table S3.

Diagnostic validation of the combination models

The combined TBR-TTP model reached an AUC of 0.79 (95% CI, 0.72–0.87) in the training cohort for the prediction

Table 2 Performance of TBR, TTP, and clinical models for the testing cohort

	TBR model	TTP model	Clinical model
AUC	0.63	0.71	0.69
AUC 95% CI	(0.47–0.78)	(0.57–0.84)	(0.50–0.86)
Accuracy	66.7%	64.3%	57.1%
Sensitivity	50.0%	50.0%	66.7%
Specificity	73.3%	70.0%	53.3%
PPV	42.9%	40.0%	36.4%
NPV	78.6%	77.8%	80.0%

CI confidence interval, TBR tumor-to-background ratio, TTP time-to-peak

of STS (Supplementary Fig. S2a, S2b), with a sensitivity of 71.4% and a specificity of 69.0%, and an AUC of 0.74 (95% CI, 0.61–0.86) in the testing cohort, with a sensitivity of 50.0% and a specificity of 70.0%.

The combined clinical-TBR model showed only slightly higher predictability of STS than the TBR model, with an AUC of 0.80 (95% CI, 0.72–0.87) in the training cohort and 0.64 (95% CI, 0.47–0.81) in the testing cohort (Fig. S2c, S2d). The sensitivity and specificity were 75.0% and 70.4% in the training cohort, and 58.3% and 60.0% in the testing cohort, respectively.

The combined clinical-TTP model showed best predictability of STS, with an AUC of 0.86 (95% CI, 0.78–0.92) in the training cohort (sensitivity 82.1% and specificity 74.7%) and 0.74 (95% CI, 0.60–0.88) in the testing cohort (sensitivity 66.7% and specificity 70.0%) (Fig. S2e, S2f).

The clinical-TBR-TTP model reached an AUC of 0.86 (95% CI, 0.70–0.93) in the training cohort for the prediction of STS (Fig. S2g, S2h), with a sensitivity of 89.3% and a specificity of 71.8%, and AUC of 0.72 (95% CI, 0.59–0.86) in the testing cohort, with a sensitivity of 58.3% and a specificity of 73.3%.

LR coefficients of the combined models are provided in Supplementary section S3. Detailed information about the performance of the combined models is shown in Table 3 and Supplementary Table S4.

Discussion

This study illustrates that integration of radiomics based on dynamic [^{18}F]FET PET may improve the assessment of short-term survival probability in patients with newly diagnosed IDH-wildtype glioblastoma. As opposed to prediction models based on clinical parameters or radiomic features alone, specifically a combined clinical-TTP model including both clinical parameters and an additional radiomic signature derived from dynamic PET accomplished a higher prognostic value for short-term survival.

Several studies have analyzed the role of [^{18}F]FET PET for the assessment of survival probability in patients with glioma [7, 8, 12, 32–35]. It has been reported that a large biological tumor volume (BTV) on static [^{18}F]FET PET [32, 33, 35] as well as a short TTP_{min} extracted from dynamic [^{18}F]FET PET at initial diagnosis are associated with STS [7, 12, 34, 35]. Besides, Bauer et al. showed that TTP_{min} is an independent prognostic factor for overall survival, reaffirming the value of dynamic [^{18}F]FET PET in the prediction of survival in glioma patients. Yet, initial radiomics data in high-grade glioma have been provided by MRI studies, achieving high AUC values for the prognostication of overall survival in the range of 0.652–0.858 in the test cohort [36–40] demonstrating that radiomics might be a valuable tool to estimate survival in brain tumor patients. Meanwhile, first promising studies have brought [^{18}F]FET PET-based radiomics into the focus: Radiomic features extracted from static [^{18}F]FET PET showed better accuracy than conventional static parameters (e.g., TBR_{max}) to identify pseudoprogression [13]. For the differentiation between radiation injury and recurrence of brain metastasis, textural features extracted from [^{18}F]FET PET had a diagnostic accuracy of 83% [41]. Carles et al. reported that [^{18}F]FET PET radiomics could contribute to the prognostic assessment [42], and Paprotka et al. established a promising tool for objective differentiation of tumor progression from treatment-related changes by combining [^{18}F]FET PET and multiparametric MRI [43]. However, those initial studies only analyzed static [^{18}F]FET PET features without taking into account important clinical parameters and, furthermore, no study so far has

Table 3 Performance of combined models for the testing cohort

Model	AUC	95% CI	Accuracy (%)	Sensitivity (%)	Specificity (%)	PPV (%)	NPV (%)
TBR-TTP	0.74	(0.61–0.86)	64.3	50.0	70.0	40.0	77.8
Clinical-TBR	0.64	(0.47–0.81)	59.5	58.3	60.0	36.8	78.3
Clinical-TTP	0.74	(0.60–0.88)	69.0	66.7	70.0	47.1	84.0
Clinical-TBR-TTP	0.72	(0.59–0.86)	69.0	58.3	73.3	46.7	81.5

CI confidence interval, TBR tumor-to-background ratio, TTP time-to-peak

utilized dynamic [^{18}F]FET PET–based radiomics to assess the probability of poor prognosis within distinct molecular brain tumor types.

The present study used clinical parameters combined with [^{18}F]FET PET radiomic features to develop combined clinical-radiomic models. A model based on clinical data only, built from six important survival-related clinical parameters, achieved an AUC of 0.69 in the independent testing cohort. A TBR model, built from two static [^{18}F]FET PET features, achieved an AUC of 0.63 in the testing cohort and thus did not perform better than the clinical model. The TTP model, however, generated from six dynamic [^{18}F]FET PET features, achieved an AUC of 0.71 in the testing cohort, thus slightly exceeding the clinical-only model and outranking the TBR-only model, highlighting the importance of dynamic PET data in the context of survival-related analyses. The combined purely imaging-based TBR-TTP model achieved only slightly better results than each model alone (AUC of 0.74 vs. AUC of 0.63 and AUC of 0.71). Eventually, the merger of the TTP radiomic signature and clinical data, resulting in the combined clinical-TTP model, achieved best predictive performance with an AUC of 0.74. Integrated discrimination improvement (IDI) was calculated between the clinical model and the combined clinical-TTP model [44]. The value of IDI was 0.1089, which was greater than 0, and the *P* value was 0.023, which was statistically significant. It indicated that the combination of TTP radiomics and clinical data, compared to clinical parameters alone, led to an improved ability of the model to identify patients at risk. Although intriguing to speculate that the clinical-TBR-TTP model would achieve highest accuracy as it includes all available information, the AUC did not improve, which may be related to the limited value of TBR information in this context, but this should be re-evaluated in larger cohorts. Taken together, as previously shown for other entities, it seems beneficial not to narrow the view to the clinical information alone when constructing a predictive model but to include radiomic signatures in clinical prediction studies as well, as the combination of clinical and radiomic information seems to be of particular value with regard to survival risk prediction [45]. When considered on its own, an AUC of 0.74 still does not seem satisfactory, as further underscored by a positive predictive value for the identification of a short-term survivor of only 47.1% even for the best model (see Table 3). From a clinical point of view, the positive and negative predictive values are highly useful metrics in the context of decision-making as they give an estimate on the correctness of a prediction. In the clinical setting, it would be particularly beneficial to identify patients at risk for short-term survival in order to facilitate the selection of more aggressive treatments or earlier inclusion in experimental treatment studies, rather

than just standard treatment, to which approximately 30% of patients do not respond. However, also the identification of long-term survivors would be helpful in the clinical routine, as pseudoprogression can occur in one-third of the patients and may, when misinterpreted as tumor progression on MRI, lead to a premature cessation of an effective treatment. Of note, while the positive predictive value was extremely low in all models, the negative predictive value, reflecting the predictability of long-term survival, reached 84% in the best model. Therefore, even though the overall accuracies of our prediction models may not yet be satisfactory for the clinical use and the low positive predictive values impede the prediction of a short-term survivor, the high negative predictive value may be helpful for clinical decision-making. Our study supports that within a neuropathologically homogenous group of aggressive IDH-wildtype glioblastomas, especially the combination of different types of information (in this case clinical data and radiomic signature) can add value to a survival prediction model and consequently hints to the potential, which lies in the inclusion of even further image-based information. Indeed, one might speculate that the addition of conventional MRI data and in a next step more sophisticated MRI data such as perfusion or diffusion-weighted MRI may further increase the power of survival risk prediction of the combined clinical-TTP model [46], but such analyses require a standardized imaging protocol to assure comparability of MRI-based radiomic features. In other tumor entities as well, especially multiparametric imaging approaches have shown highly promising results for survival prediction, e.g., reaching an accuracy of up to 98% in a study on cervical cancer as compared to only 56–60% for prediction models using the standard clinical variables alone [47, 48]. Accordingly, dual PET imaging studies including other tracers than [^{18}F]FET in IDH-wildtype glioblastoma, such as TSPO-ligands which offer complementary information to the [^{18}F]FET uptake [49], are of high potential to further increase the power of survival prediction models, as exemplified by recent successful multi-tracer PET prediction approaches in other entities, such as prostate cancer [50].

Although the number of patients included in the current study is by far higher than in most previous [^{18}F]FET PET radiomics studies, a further increase in patient numbers may in future result in outperforming radiomics-only based approaches, as already shown in large-scale analyses for other medical settings [51]. According to the above-generated multivariate LR-based formulas, the known risk factors of high WHO grade, unmethylated MGMT promoter, TERTp mutation as well as higher patient age and lower KPS at diagnosis of IDH-wildtype glioblastoma were more likely associated with short-term survival [52–55]. However, gender has different correlations in different formulas, which

is inconsistent with the literature [53], although the weight of this parameter was low. This may likewise be due to the relatively low number of patients included in this study.

Whereas, in clinical routine, established dynamic [^{18}F]FET PET parameters such as the time–activity curve and/or the slope are usually only derived from representative sub-volumes of interest within the tumor [7, 9, 56], in the current study every single voxel of the tumor was analyzed in order to generate whole-tumor TTP maps of dynamic [^{18}F]FET PET images. This comprehensive whole-tumor approach facilitated radiomic features extraction in dynamic image data and ensured to account for heterogeneity of uptake kinetics which has a major clinical impact when assessing brain tumors in dynamic [^{18}F]FET PET [57]. In this context, a relationship between tumor heterogeneity and the STS group could be found in the feature *ClusterProminence (CP)*. CP belongs to the *Gray Level Co-occurrence Matrix (GLCM)* and measures the skewness and asymmetry of the GLCM. A higher value implies more asymmetry while a lower value indicates a peak near the mean value and less variation around the mean. This correlation with the STS group indicates that a patient with a heterogeneous tumor in dynamic [^{18}F]FET PET images is more likely to be identified as high-risk patient for short-term survival. Another exemplary radiomic feature, which is associated with the STS group, is *Maximum 3D diameter, 3D shape feature*. The latter is defined as the largest pairwise Euclidean distance between tumor surface mesh vertices. This correlation, in simplified terms, indicates that patients belonging to the STS group have a tumor that shows large spread on PET. This finding is consistent with the literature—large tumor volumes on [^{18}F]FET PET were reported to be associated with poor overall survival in glioblastoma patients before radiation therapy with concomitant and adjuvant temozolomide [32, 33]. Details of other features are shown in the Supplementary information.

There are several limitations to this study. Only single-center data have been investigated, which led to the relatively small sample size and the lack of external validation. Yet, only single-center data have been chosen in this study since dynamic [^{18}F]FET PET is not always acquired routinely in other centers and pooling PET data with differences in time framing, image reconstruction algorithm, and scanner type may require prior implementation and validation of, e.g., feature harmonization procedures [58]. Moreover, it should be noted that almost all previous [^{18}F]FET PET radiomics studies have been performed with much smaller numbers of cases. The reliability of the reported scores was additionally evaluated using nested cross-validation [59] with five random splits in the outer loop, yielding a high AUC variability of 10% for the TTP model, 15% for the TBR model, and 11% for the clinical model (Supplementary material S4). Thereby,

different radiomic signatures were obtained for each split of the outer loop since feature selection and model building are not robust when dealing with small sample sizes. Feature selection represents a challenge and has an impact on the performance of prediction models. Other feature selection methods comprise, e.g., filter methods such as minimum redundancy maximum relevance (MRMR) or ensemble methods, which provide a good balance between robust feature selection and model performance. Wrapper methods such as RFE have the advantage that feature dependencies can be modeled and that they interact with the classifier, while also bearing the risk of overfitting [60]. To enable standardized segmentation of tumor regions, only positive [^{18}F]FET PET images were included. Furthermore, MRI-based radiomics, as a more widely established and complementary tool, were not included in this study. Future studies may benefit from the combined use of multiparametric MRI data.

Conclusion

This study built and evaluated prediction models for survival combining both radiomic features extracted from static and dynamic [^{18}F]FET PET and clinical parameters. Specifically, the combination of clinical parameters with radiomics based on dynamic [^{18}F]FET PET data achieved a higher prognostic accuracy for the individualized assessment of short-term survival in patients with newly diagnosed IDH-wildtype glioblastoma in comparison to models using conventional clinical parameters only. Although the final accuracy remained moderate, the integration of dynamic [^{18}F]FET PET radiomic data into clinical prediction models may improve patient stratification beyond established prognostic markers. Future prospective radiomic studies using multimodal imaging data are needed to evaluate whether the integration of additional imaging parameters may further improve the prognostic performance and enhance the clinical interpretation of the study results.

Supplementary Information The online version contains supplementary material available at <https://doi.org/10.1007/s00259-022-05988-2>.

Author contribution Conceptualization: ZL, NLA, and LK. Data acquisition: AH, LMU, VCR, SQ, LMB, BS, and MU. Image processing: LK. Implementation and application of the software for generation of parametric maps and for radiomic feature extraction using Pyradiomics: LK. Feature selection and machine learning implementation and application: ZL. Formal analysis: AH. Writing—original draft preparation: ZL, AH, NLA, and LK. Writing—review and editing: all authors. Funding acquisition: ZL and NLA. Supervision: PB, J-CT, NLA, and LK. All authors have read and agreed to the published version of the manuscript.

Funding Open Access funding enabled and organized by Projekt DEAL. This work was supported by the Collaborative Research Centre SFB-824 and the Research Group 2858 (project number 421887978) of the Deutsche Forschungsgemeinschaft (DFG), and by the Else Kröner-Fresenius-Stiftung. The China Scholarship Council (CSC) funded this study for ZL.

Data availability The data that support the findings of this study are available on request from the corresponding author, ZL. The data are not publicly available due to the privacy of research participants.

Code availability The code that support the findings of this study are available from ZL and LK on reasonable request.

Declarations

Ethics approval Ethical approval of the retrospective data analysis was given by the institutional review board of the LMU (#606–16) in accordance with the ICH Guideline for Good Clinical Practice (GCP) and the declaration of Helsinki.

Consent to participate All patients have given written informed consent prior to the PET examination.

Conflict of interest The authors declare no competing interests.

Open Access This article is licensed under a Creative Commons Attribution 4.0 International License, which permits use, sharing, adaptation, distribution and reproduction in any medium or format, as long as you give appropriate credit to the original author(s) and the source, provide a link to the Creative Commons licence, and indicate if changes were made. The images or other third party material in this article are included in the article's Creative Commons licence, unless indicated otherwise in a credit line to the material. If material is not included in the article's Creative Commons licence and your intended use is not permitted by statutory regulation or exceeds the permitted use, you will need to obtain permission directly from the copyright holder. To view a copy of this licence, visit <http://creativecommons.org/licenses/by/4.0/>.

References


- Louis DN, Perry A, Reifenberger G, von Deimling A, Figarella-Branger D, Cavenee WK, et al. The 2016 World Health Organization Classification of Tumors of the Central Nervous System: a summary. *Acta Neuropathol.* 2016;131:803–20. <https://doi.org/10.1007/s00401-016-1545-1>.
- Louis DN, Perry A, Wesseling P, Brat DJ, Cree IA, Figarella-Branger D, et al. The 2021 WHO Classification of Tumors of the Central Nervous System: a summary. *Neuro Oncol.* 2021;23:1231–51. <https://doi.org/10.1093/neuonc/noab106>.
- Tan AC, Ashley DM, López GY, Malinzak M, Friedman HS, Khasraw M. Management of glioblastoma: state of the art and future directions. *CA Cancer J Clin.* 2020;70:299–312. <https://doi.org/10.3322/caac.21613>.
- Esteller M, Garcia-Foncillas J, Andion E, Goodman SN, Hidalgo OF, Vanaclocha V, et al. Inactivation of the DNA-repair gene MGMT and the clinical response of gliomas to alkylating agents. *N Engl J Med.* 2000;343:1350–4. <https://doi.org/10.1056/nejm200011093431901>.
- Van Meir EG, Hadjipanayis CG, Norden AD, Shu HK, Wen PY, Olson JJ. Exciting new advances in neuro-oncology: the avenue to a cure for malignant glioma. *CA Cancer J Clin.* 2010;60:166–93. <https://doi.org/10.3322/caac.20069>.
- Pace A, Dirven L, Koekkoek JAF, Golla H, Fleming J, Rudà R, et al. European Association for Neuro-Oncology (EANO) guidelines for palliative care in adults with glioma. *Lancet Oncol.* 2017;18:e330–e40. [https://doi.org/10.1016/s1470-2045\(17\)30345-5](https://doi.org/10.1016/s1470-2045(17)30345-5).
- Jansen NL, Suchorska B, Wenter V, Schmid-Tannwald C, Todica A, Eigenbrod S, et al. Prognostic significance of dynamic 18F-FET PET in newly diagnosed astrocytic high-grade glioma. *J Nucl Med.* 2015;56:9–15. <https://doi.org/10.2967/jnumed.114.144675>.
- Jansen NL, Suchorska B, Wenter V, Eigenbrod S, Schmid-Tannwald C, Zwergal A, et al. Dynamic 18F-FET PET in newly diagnosed astrocytic low-grade glioma identifies high-risk patients. *J Nucl Med.* 2014;55:198–203. <https://doi.org/10.2967/jnumed.113.122333>.
- Pöppel G, Kreth FW, Mehrkens JH, Herms J, Seelos K, Koch W, et al. FET PET for the evaluation of untreated gliomas: correlation of FET uptake and uptake kinetics with tumour grading. *Eur J Nucl Med Mol Imaging.* 2007;34:1933–42. <https://doi.org/10.1007/s00259-007-0534-y>.
- Albert NL, Weller M, Suchorska B, Galldiks N, Soffietti R, Kim MM, et al. Response Assessment in Neuro-Oncology working group and European Association for Neuro-Oncology recommendations for the clinical use of PET imaging in gliomas. *Neuro Oncol.* 2016;18:1199–208. <https://doi.org/10.1093/neuonc/now058>.
- Kunz M, Albert NL, Unterrainer M, la Fougere C, Egensperger R, Schuller U, et al. Dynamic 18F-FET PET is a powerful imaging biomarker in gadolinium-negative gliomas. *Neuro Oncol.* 2019;21:274–84. <https://doi.org/10.1093/neuonc/noy098>.
- Bauer EK, Stoffels G, Blau T, Reifenberger G, Felsberg J, Werner JM, et al. Prediction of survival in patients with IDH-wildtype astrocytic gliomas using dynamic O-(2-[(18)F]-fluoroethyl)-L-tyrosine PET. *Eur J Nucl Med Mol Imaging.* 2020;47:1486–95. <https://doi.org/10.1007/s00259-020-04695-0>.
- Lohmann P, Elahmadawy MA, Gutsche R, Werner JM, Bauer EK, Cecon G, et al. FET PET radiomics for differentiating pseudoprogression from early tumor progression in glioma patients post-chemoradiation. *Cancers (Basel).* 2020;12. <https://doi.org/10.3390/cancers12123835>.
- Li Z, Kaiser L, Holzgreve A, Ruf VC, Suchorska B, Wenter V, et al. Prediction of TERTp-mutation status in IDH-wildtype high-grade gliomas using pre-treatment dynamic [(18)F]FET PET radiomics. *Eur J Nucl Med Mol Imaging.* 2021. <https://doi.org/10.1007/s00259-021-05526-6>.
- Stupp R, Hegi ME, Mason WP, van den Bent MJ, Taphoorn MJ, Janzer RC, et al. Effects of radiotherapy with concomitant and adjuvant temozolomide versus radiotherapy alone on survival in glioblastoma in a randomised phase III study: 5-year analysis of the EORTC-NCIC trial. *Lancet Oncol.* 2009;10:459–66. [https://doi.org/10.1016/s1470-2045\(09\)70025-7](https://doi.org/10.1016/s1470-2045(09)70025-7).
- Zhang X, Lu H, Tian Q, Feng N, Yin L, Xu X, et al. A radiomics nomogram based on multiparametric MRI might stratify glioblastoma patients according to survival. *Eur Radiol.* 2019;29:5528–38. <https://doi.org/10.1007/s00330-019-06069-z>.
- Langen KJ, Bartenstein P, Boecker H, Brust P, Coenen HH, Drzezga A, et al. German guidelines for brain tumour imaging by PET and SPECT using labelled amino acids. *Nuklearmedizin.* 2011;50:167–73. <https://doi.org/10.3413/nuk-2011041>.
- Unterrainer M, Vettermann F, Brendel M, Holzgreve A, Lifschitz M, Zahringer M, et al. Towards standardization of 18F-FET PET imaging: do we need a consistent method of background activity assessment? *EJNMMI Res.* 2017;7:48.
- Law I, Albert NL, Arbizu J, Boellaard R, Drzezga A, Galldiks N, et al. Joint EANM/EANO/RANO practice guidelines/SNMMI procedure standards for imaging of gliomas using PET with radiolabelled amino acids and [(18)F]FDG: version 1.0. *Eur J Nucl Med Mol Imaging.* 2019;46:540–57. <https://doi.org/10.1007/s00259-018-4207-9>.

20. Pauleit D, Floeth F, Hamacher K, Riemenschneider MJ, Reifenberger G, Muller HW, et al. O-(2-[¹⁸F]fluoroethyl)-L-tyrosine PET combined with MRI improves the diagnostic assessment of cerebral gliomas. *Brain*. 2005;128:678–87. <https://doi.org/10.1093/brain/awh399>.
21. Vomacka L, Unterrainer M, Holzgreve A, Mille E, Gosewisch A, Brosch J, et al. Voxel-wise analysis of dynamic 18F-FET PET: a novel approach for non-invasive glioma characterisation. *EJNMMI Res*. 2018;8:91. <https://doi.org/10.1186/s13550-018-0444-y>.
22. Van Griethuysen JJM, Fedorov A, Parmar C, Hosny A, Aucoin N, Narayan V, et al. Computational radiomics system to decode the radiographic phenotype. *Can Res*. 2017;77:e104–7. <https://doi.org/10.1158/0008-5472.can-17-0339>.
23. Zwanenburg A, Vallières M, Abdalah MA, Aerts H, Andrearczyk V, Apte A, et al. The image biomarker standardization initiative: standardized quantitative radiomics for high-throughput image-based phenotyping. *Radiology*. 2020;295:328–38. <https://doi.org/10.1148/radiol.2020191145>.
24. Leijenaar RT, Nalbantov G, Carvalho S, van Elmpt WJ, Troost EG, Boellaard R, et al. The effect of SUV discretization in quantitative FDG-PET radiomics: the need for standardized methodology in tumor texture analysis. *Sci Rep*. 2015;5:11075. <https://doi.org/10.1038/srep11075>.
25. Kaiser LGM, Ahmadi SA, Unterrainer M, Holzgreve A, Mille E, Gosewisch A, Brosch J, Suchorska B, Navab N, Tonn JC, Ziegler S, Bartenstein P, Albert NL, Böning G. Annual Congress of the European Association of Nuclear Medicine October 12–16, 2019 Barcelona, Spain. *Eur J Nucl Med Mol Imaging*. 2019;46:1–952. <https://doi.org/10.1007/s00259-019-04486-2>.
26. Song Y, Zhang J, Zhang Y-D, Hou Y, Yan X, Wang Y, et al. FeAture Explorer (FAE): a tool for developing and comparing radiomics models. *PLoS ONE*. 2020;15:e0237587. <https://doi.org/10.1371/journal.pone.0237587>.
27. Pedregosa F, Varoquaux G, Gramfort A, Michel V, Thirion B, Grisel O, et al. Scikit-learn: machine learning in Python. *J Mach Learn Res*. 2011;12:2825–30.
28. Tomz M, King G, Zeng L. ReLogit: rare events logistic regression. 2003. 2003;8:27. <https://doi.org/10.18637/jss.v008.i02>.
29. Cohen I, Huang Y, Chen J, Benesty J. Noise reduction in speech processing. *Springer topics in signal processing*. Springer Berlin Heidelberg; 2009.
30. Chen C, Qin Y, Cheng J, Gao F, Zhou X. Texture analysis of fat-suppressed T2-weighted magnetic resonance imaging and use of machine learning to discriminate nasal and paranasal sinus small round malignant cell tumors. *Front Oncol*. 2021;11:701289. <https://doi.org/10.3389/fonc.2021.701289>.
31. Granitto PM, Furlanello C, Biasioli F, Gasperi F. Recursive feature elimination with random forest for PTR-MS analysis of agroindustrial products. *Chemom Intell Lab Syst*. 2006;83:83–90. <https://doi.org/10.1016/j.chemolab.2006.01.007>.
32. Suchorska B, Jansen NL, Linn J, Kretzschmar H, Janssen H, Eigenbrod S, et al. Biological tumor volume in 18F-FET-PET before radiochemotherapy correlates with survival in GBM. *Neurology*. 2015;84:710–9. <https://doi.org/10.1212/wnl.0000000000001262>.
33. Poulsen SH, Urup T, Grunnet K, Christensen IJ, Larsen VA, Jensen ML, et al. The prognostic value of FET PET at radiotherapy planning in newly diagnosed glioblastoma. *Eur J Nucl Med Mol Imaging*. 2017;44:373–81. <https://doi.org/10.1007/s00259-016-3494-2>.
34. Suchorska B, Giese A, Biczok A, Unterrainer M, Weller M, Drexler M, et al. Identification of time-to-peak on dynamic 18F-FET-PET as a prognostic marker specifically in IDH1/2 mutant diffuse astrocytoma. *Neuro Oncol*. 2018;20:279–88. <https://doi.org/10.1093/neuonc/nox153>.
35. Mittlmeier LM, Suchorska B, Ruf V, Holzgreve A, Brendel M, Herms J, et al. (18)F-FET PET Uptake characteristics of long-term IDH-wildtype diffuse glioma survivors. *Cancers (Basel)*. 2021;13. <https://doi.org/10.3390/cancers13133163>.
36. Zhang X, Lu D, Gao P, Tian Q, Lu H, Xu X, et al. Survival-relevant high-risk subregion identification for glioblastoma patients: the MRI-based multiple instance learning approach. *Eur Radiol*. 2020;30:5602–10. <https://doi.org/10.1007/s00330-020-06912-8>.
37. Bae S, Choi YS, Ahn SS, Chang JH, Kang SG, Kim EH, et al. Radiomic MRI phenotyping of glioblastoma: improving survival prediction. *Radiology*. 2018;289:797–806. <https://doi.org/10.1148/radiol.2018180200>.
38. Liao X, Cai B, Tian B, Luo Y, Song W, Li Y. Machine-learning based radiogenomics analysis of MRI features and metagenes in glioblastoma multiforme patients with different survival time. *J Cell Mol Med*. 2019;23:4375–85. <https://doi.org/10.1111/jcmm.14328>.
39. Choi Y, Nam Y, Jang J, Shin NY, Lee YS, Ahn KJ, et al. Radiomics may increase the prognostic value for survival in glioblastoma patients when combined with conventional clinical and genetic prognostic models. *Eur Radiol*. 2021;31:2084–93. <https://doi.org/10.1007/s00330-020-07335-1>.
40. Xu Y, He X, Li Y, Pang P, Shu Z, Gong X. The nomogram of MRI-based radiomics with complementary visual features by machine learning improves stratification of glioblastoma patients: a multicenter study. *J Magn Reson Imaging*. 2021;54:571–83. <https://doi.org/10.1002/jmri.27536>.
41. Lohmann P, Kocher M, Ceccon G, Bauer EK, Stoffels G, Viswanathan S, et al. Combined FET PET/MRI radiomics differentiates radiation injury from recurrent brain metastasis. *Neuroimage Clin*. 2018;20:537–42. <https://doi.org/10.1016/j.nicl.2018.08.024>.
42. Carles M, Popp I, Starke MM, Mix M, Urbach H, Schimek-Jasch T, et al. FET-PET radiomics in recurrent glioblastoma: prognostic value for outcome after re-irradiation? *Radiat Oncol (London, England)*. 2021;16:46. <https://doi.org/10.1186/s13014-020-01744-8>.
43. Paprottka KJ, Kleiner S, Preibisch C, Kofler F, Schmidt-Graf F, Delbridge C, et al. Fully automated analysis combining [(18)F]-FET-PET and multiparametric MRI including DSC perfusion and APTw imaging: a promising tool for objective evaluation of glioma progression. *Eur J Nucl Med Mol Imaging*. 2021;48:4445–55. <https://doi.org/10.1007/s00259-021-05427-8>.
44. Pencina MJ, D'Agostino RB Sr, D'Agostino RB Jr, Vasan RS. Evaluating the added predictive ability of a new marker: from area under the ROC curve to reclassification and beyond. *Stat Med*. 2008;27:157–72. <https://doi.org/10.1002/sim.2929> (discussion 207–12).
45. Huang YQ, Liang CH, He L, Tian J, Liang CS, Chen X, et al. Development and validation of a radiomics nomogram for preoperative prediction of lymph node metastasis in colorectal cancer. *J Clin Oncol*. 2016;34:2157–64. <https://doi.org/10.1200/jco.2015.65.9128>.
46. Galldiks N, Zadeh G, Lohmann P. Artificial intelligence, radiomics, and deep learning in neuro-oncology. *Neurooncol Adv*. 2020;2:iv1–2. <https://doi.org/10.1093/noajnl/vdaa179>.
47. Lucia F, Visvikis D, Desseroit MC, Miranda O, Malhaire JP, Robin P, et al. Prediction of outcome using pretreatment (18)F-FDG PET/CT and MRI radiomics in locally advanced cervical cancer treated with chemoradiotherapy. *Eur J Nucl Med Mol Imaging*. 2018;45:768–86. <https://doi.org/10.1007/s00259-017-3898-7>.
48. Lucia F, Visvikis D, Vallières M, Desseroit MC, Miranda O, Robin P, et al. External validation of a combined PET and MRI radiomics model for prediction of recurrence in cervical cancer patients treated with chemoradiotherapy. *Eur J Nucl Med Mol Imaging*. 2019;46:864–77. <https://doi.org/10.1007/s00259-018-4231-9>.

49. Unterrainer M, Fleischmann DF, Diekmann C, Vomacka L, Lindner S, Vettermann F, et al. Comparison of (18)F-GE-180 and dynamic (18)F-FET PET in high grade glioma: a double-tracer pilot study. *Eur J Nucl Med Mol Imaging*. 2019;46:580–90. <https://doi.org/10.1007/s00259-018-4166-1>.
50. Michalski K, Ruf J, Goetz C, Seitz AK, Buck AK, Lapa C, et al. Prognostic implications of dual tracer PET/CT: PSMA ligand and [(18)F]FDG PET/CT in patients undergoing [(177)Lu]PSMA radioligand therapy. *Eur J Nucl Med Mol Imaging*. 2021;48:2024–30. <https://doi.org/10.1007/s00259-020-05160-8>.
51. Esteve A, Kuprel B, Novoa RA, Ko J, Swetter SM, Blau HM, et al. Dermatologist-level classification of skin cancer with deep neural networks. *Nature*. 2017;542:115–8. <https://doi.org/10.1038/nature21056>.
52. Reifenberger G, Weber RG, Riehmer V, Kaulich K, Willscher E, Wirth H, et al. Molecular characterization of long-term survivors of glioblastoma using genome-and transcriptome-wide profiling. *Int J Cancer*. 2014;135:1822–31.
53. Burgenske DM, Yang J, Decker PA, Kollmeyer TM, Kosel ML, Mladek AC, et al. Molecular profiling of long-term IDH-wildtype glioblastoma survivors. *Neuro Oncol*. 2019;21:1458–69.
54. Park JK, Hodges T, Arko L, Shen M, Iacono DD, McNabb A, et al. Scale to predict survival after surgery for recurrent glioblastoma multiforme. *J Clin Oncol*. 2010;28:3838.
55. Simon M, Hosen I, Gousias K, Rachakonda S, Heidenreich B, Gessi M, et al. TERT promoter mutations: a novel independent prognostic factor in primary glioblastomas. *Neuro Oncol*. 2015;17:45–52. <https://doi.org/10.1093/neuonc/nou158>.
56. Jansen NL, Graute V, Armbruster L, Suchorska B, Lutz J, Eigenbrod S, et al. MRI-suspected low-grade glioma: is there a need to perform dynamic FET PET? *Eur J Nucl Med Mol Imaging*. 2012;39:1021–9. <https://doi.org/10.1007/s00259-012-2109-9>.
57. Kunz M, Thon N, Eigenbrod S, Hartmann C, Egensperger R, Herms J, et al. Hot spots in dynamic (18)FET-PET delineate malignant tumor parts within suspected WHO grade II gliomas. *Neuro Oncol*. 2011;13:307–16. <https://doi.org/10.1093/neuonc/noq196>.
58. Da-Ano R, Masson I, Lucia F, Doré M, Robin P, Alfieri J, et al. Performance comparison of modified ComBat for harmonization of radiomic features for multicenter studies. *Sci Rep*. 2020;10:10248. <https://doi.org/10.1038/s41598-020-66110-w>.
59. Varma S, Simon R. Bias in error estimation when using cross-validation for model selection. *BMC Bioinformatics*. 2006;7:91. <https://doi.org/10.1186/1471-2105-7-91>.
60. Saeys Y, Inza I, Larranaga P. A review of feature selection techniques in bioinformatics. *Bioinformatics*. 2007;23:2507–17. <https://doi.org/10.1093/bioinformatics/btm344>.

Publisher's note Springer Nature remains neutral with regard to jurisdictional claims in published maps and institutional affiliations.

Authors and Affiliations

Zhichong Li¹  · Adrien Holzgreve¹ · Lena M. Unterrainer¹ · Viktoria C. Ruf² · Stefanie Quach³ · Laura M. Bartos¹ · Bogdana Suchorska^{3,4} · Maximilian Niyazi^{5,6} · Vera Wenter¹ · Jochen Herms² · Peter Bartenstein^{1,6} · Joerg-Christian Tonn^{3,6} · Marcus Unterrainer⁷ · Nathalie L. Albert^{1,6} · Lena Kaiser¹

¹ Department of Nuclear Medicine, University Hospital, LMU Munich, Marchioninstr. 15, 81377 Munich, Germany

² Center for Neuropathology and Prion Research, LMU Munich, Munich, Germany

³ Department of Neurosurgery, University Hospital, LMU Munich, Munich, Germany

⁴ Department of Neurosurgery, Sana Hospital, Duisburg, Germany

⁵ Department of Radiotherapy, University Hospital, LMU Munich, Munich, Germany

⁶ German Cancer Consortium (DKTK), Partner Site Munich, German Cancer Research Center (DKFZ), Heidelberg, Germany

⁷ Department of Radiology, University Hospital, LMU Munich, Munich, Germany